

Collective electronic excitations in charge density wave systems: The case of CuTe

Pierluigi Cudazzo and Ludger Wirtz

*Department of Physics and Materials Science, University of Luxembourg, 162a avenue de la Faïencerie, L-1511 Luxembourg, Luxembourg
and European Theoretical Spectroscopy Facility (ETSF)*



(Received 18 May 2021; revised 18 July 2021; accepted 17 August 2021; published 1 September 2021)

The study of neutral electronic excitations directly probed by electron energy loss spectroscopy experiments allows obtaining important insight about the physical origin of the charge density wave (CDW) transition in solids. In particular it allows us to disentangle purely phononic mechanisms from the excitonic insulator scenario which is associated to a purely electronic mechanism. As a matter of fact, while the loss function of the excitonic insulators should display negative dispersive features associated to the softening of neutral electronic excitations at the CDW wave vector above the critical temperature, no softening is expected when the driving force is purely phononic. Here we perform a microscopic analysis of the dynamical charge response of CuTe, a material that displays a low-temperature Peierls-like CDW instability. By means of first-principles time-dependent density functional calculations of the loss function, we characterize the plasmon dispersion along the different directions, highlighting the role of the intrinsic structural anisotropy and the effects of the crystal local fields that are responsible for the periodic reappearance of the spectra of the first Brillouin zone as well as the formation of an acousticlike plasmon. Finally, we demonstrate that also in this system, in analogy with other materials displaying excitonic insulator instability, the low energy region of the loss function presents negative dispersive structures at momentum transfer close to the CDW wave vector. This is a feature common to both excitonic insulator transition and Peierls distortion that further highlights how the difference between the two mechanisms is at most quantitative.

DOI: [10.1103/PhysRevB.104.125101](https://doi.org/10.1103/PhysRevB.104.125101)

I. INTRODUCTION

Charge-density-wave (CDW) states in low-dimensional electronic systems are among the most actively studied phenomena in condensed matter physics [1,2]. The experimental consequences of the CDW order include the appearance of a lattice distortion, the softening of phonon modes, and the appearance of an excitation gap in the single-particle spectrum. An intense debate has been created over the years about the origin of the CDW phase transition in the different materials. Several explanations have been put forward: from purely electronic mechanisms such as Fermi surface nestings [3], van Hove singularities (saddle points) in the density of states (DOS) [4], and excitonic effects [5] to electron-phonon coupling [6,7] and Jahn-Teller distortion [8]. Among them, the excitonic insulator picture [5] which is tightly linked with the Bose-Einstein condensation phenomena is probably the most appealing one. Here due to the attractive electron-hole interaction induced by exchange-correlation effects, spontaneous bound electron-hole pairs (excitons) with a given wave vector can be formed at zero energy cost if the exciton binding energy is large enough. Excitons being bosonic like excitations, they can condensate below a given critical temperature in analogy with the Cooper pairs in superconductivity. The new ground state is characterized by a CDW order with periodicity set by the exciton wave vector and by a change of the electronic band structure. In addition, the electric field caused by the

CDW in general leads to the displacement of the positive ions from their ideal equilibrium positions giving rise to a periodic lattice distortion.

Nevertheless, despite the large efforts in the search of the excitonic insulator state, a conclusive experimental evidence for the existence of this phase remains elusive. This happens because an excitonic insulator is extremely difficult to disentangle from the Peierls distortion [9] which is characterized by the same outcome: a novel ground state with lower symmetry exhibiting a CDW, a periodic lattice distortion, and a gap in the electronic band structure. In this case the CDW order arises from the cooperation between the electron-phonon coupling and the strong enhancement of the electronic susceptibility at the CDW wave vector often ascribed to the Fermi surface nesting. The interplay of the two effects gives rise to the complete softening of a phonon mode (large Kohn anomaly) [10] that results in a lattice distortion.

The dynamical charge-density response is a key quantity for setting the CDW in both excitonic insulator and Peierls mechanisms, because it provides the renormalization of the electron-hole and electron-phonon interactions. Thus, its investigation is of utmost importance for understanding the electronic properties of CDW systems. Moreover it contains all the information about the neutral electronic excitations that are strongly affected by the CDW order. For example, quantum fluctuations associated to the CDW enhance the damping of the collective excitations (plasmons) and push them to

higher energy due to the presence of a CDW gap [11]. The discovery of an unusual negative plasmon dispersion in several CDW materials above the critical temperature drove different authors to ascribe this behavior to the CDW instability [12–14]. This is seemingly in contrast with the common idea that the softening of low energy incoherent excitations such as excitons or electron-hole pairs and not plasmons should be a peculiarity of purely electronically unstable systems (i.e., the excitonic insulators) [15–19] and is considered as experimental evidence that allows disentangling the excitonic insulator from the Peierls transition [18].

In this paper, in order to better understand the relation between the CDW instability and the dispersion of neutral electronic excitations, we performed an extensive study of the charge-density response in CuTe, a material that, as observed in recent angle resolved photoemission spectroscopy (ARPES) experiments [20], displays a CDW order below 335 K. In particular, first principles density functional theory (DFT) calculations of the electronic structure and phonon dispersion demonstrated that the CDW order is induced by the interplay between electron-phonon coupling and a strong enhancement of the electronic susceptibility at the CDW wave vector \mathbf{q}_N [20,21]. The latter has been ascribed to the presence of a nested Fermi surface arising from the quasi 1D electronic structure. All these features suggest that the CDW in this system is a Peierls-like transition.

Our study reveals that, in general, the plasmon softening is not related to the CDW instability but that it is a pure band effect common to both CDW systems as well as materials that do not display CDW transition. As a matter of fact, the plasmon dispersion is not only set by the behavior of the metallic bands involved in the CDW pairing but strongly depends on high-energy interband transitions [22] that are weakly affected by the CDW ordering. On the other hand, the CDW instability is tightly linked with the presence of negative dispersive structures in the low energy region of the loss function associated to incoherent excitations such as excitons or electron-hole pairs. However, this behavior is a feature common to both the excitonic insulator transition and the Peierls distortion. Finally, we characterize the plasmon dispersion along the different crystal directions, highlighting the role of the intrinsic structural anisotropy and the effect of the crystal local fields that are responsible for the periodic reappearance of the spectra of the first Brillouin zone as well as for the formation of an acousticlike plasmon [23].

This paper is organized as follows: In Sec. II we summarize the computational method while in Sec. III, after a brief overview of the electronic and structural properties of CuTe, we will analyze the behavior of the high energy plasmonic excitations. The last part of this section is focused on the low energy excitations and their link with the CDW instability. Finally the last section is devoted to the conclusions.

II. THEORETICAL FRAMEWORK AND COMPUTATIONAL DETAILS

In the present work, the key quantity is the loss function $L(\mathbf{q}, \omega) = -\text{Im}\epsilon_M^{-1}(\mathbf{q}, \omega)$, where \mathbf{q} is the momentum transfer, which can be measured by electron energy loss spectroscopy

(EELS) or inelastic x ray scattering (IXS). The loss function can be written in terms of the real and imaginary parts of the macroscopic dielectric function $\epsilon_M = \epsilon_1 + i\epsilon_2$:

$$L(\mathbf{q}, \omega) = \frac{\epsilon_2(\mathbf{q}, \omega)}{[\epsilon_1(\mathbf{q}, \omega)]^2 + [\epsilon_2(\mathbf{q}, \omega)]^2}. \quad (1)$$

In particular, plasmon resonances correspond to zeros of ϵ_1 where the damping given by ϵ_2 is not too large. On the other hand, ϵ_2 defines the incoherent part of L . It is associated to the excitons and to the incoherent superpositions of electron-hole pairs and dominates the loss function when ϵ_1 is weakly frequency dependent and very large with respect to ϵ_2 .

In the theoretical simulations [24], the macroscopic dielectric function $\epsilon_M(\mathbf{q}, \omega)$ is obtained from the microscopic dielectric function $\epsilon_{\mathbf{G}, \mathbf{G}'}(\mathbf{q}_r, \omega)$ as:

$$\epsilon_M(\mathbf{q}_r + \mathbf{G}, \omega) = \frac{1}{\epsilon_{\mathbf{G}, \mathbf{G}}^{-1}(\mathbf{q}_r, \omega)}, \quad (2)$$

where \mathbf{G} is a reciprocal-lattice vector and \mathbf{q}_r belongs to the first Brillouin zone such that $\mathbf{q} = \mathbf{q}_r + \mathbf{G}$. The microscopic dielectric function is directly linked to the charge-density response function χ :

$$\epsilon_{\mathbf{G}, \mathbf{G}}^{-1}(\mathbf{q}_r, \omega) = \delta_{\mathbf{G}, \mathbf{G}'} + v_c(\mathbf{q}_r + \mathbf{G})\chi_{\mathbf{G}, \mathbf{G}'}(\mathbf{q}_r, \omega). \quad (3)$$

Within linear-response time-dependent density-functional theory (TDDFT) [25], χ is calculated from the solution of a Dyson-like equation connecting χ with its independent-particle counterpart χ_0 :

$$\begin{aligned} \chi_{\mathbf{G}, \mathbf{G}'}(\mathbf{q}_r, \omega) &= \chi_{\mathbf{G}, \mathbf{G}'}^0(\mathbf{q}_r, \omega) + \sum_{\mathbf{G}_1, \mathbf{G}_2} \chi_{\mathbf{G}, \mathbf{G}_1}^0(\mathbf{q}_r, \omega) \\ &\times [v_c(\mathbf{q}_r + \mathbf{G}_1)\delta_{\mathbf{G}_1, \mathbf{G}_2} + f_{\mathbf{G}_1, \mathbf{G}_2}^{xc}(\mathbf{q}_r, \omega)] \\ &\times \chi_{\mathbf{G}_2, \mathbf{G}'}(\mathbf{q}_r, \omega). \end{aligned} \quad (4)$$

Here χ_0 is built from ground-state Kohn-Sham (KS) eigenvalues $\varepsilon_{n\mathbf{k}}$ and orbitals $\phi_{n\mathbf{k}}$ (with Fermi occupations $f_{n\mathbf{k}}$, volume Ω and $\eta \rightarrow 0^+$):

$$\begin{aligned} \chi_{\mathbf{G}, \mathbf{G}'}^0(\mathbf{q}_r, \omega) &= \frac{1}{\Omega} \sum_{n, n', \mathbf{k}} \frac{f_{n\mathbf{k}} - f_{n'\mathbf{k}+\mathbf{q}_r}}{\omega + \varepsilon_{n\mathbf{k}} - \varepsilon_{n'\mathbf{k}+\mathbf{q}_r} + i\eta} \\ &\times \langle \phi_{n\mathbf{k}} | e^{-i(\mathbf{q}_r + \mathbf{G}) \cdot \mathbf{r}} | \phi_{n'\mathbf{k}+\mathbf{q}_r} \rangle \\ &\times \langle \phi_{n\mathbf{k}} | e^{-i(\mathbf{q}_r + \mathbf{G}') \cdot \mathbf{r}} | \phi_{n'\mathbf{k}+\mathbf{q}_r} \rangle \end{aligned} \quad (5)$$

and f_{xc} is the TDDFT kernel which has to be approximated. Setting $f_{xc} = 0$ corresponds to the random-phase approximation (RPA).

We calculated the ground state of CuTe using the DFT framework with the local-density approximation (LDA) for the exchange-correlation functional [26]. We adopted the experimental crystal structure from Ref. [20]. We employed the plane-wave basis approach of the QUANTUM ESPRESSO code [27] with norm-conserving Vanderbilt pseudopotentials [28]. Ground-state calculations converged with a 140 Ry cutoff. For the linear-response calculations of the loss functions we used YAMBO [29] and a $50 \times 40 \times 20$ k -point grid in the conventional unit cell. We adopted the RPA in all calculations discussed in the following, since exchange-correlation effects within the adiabatic local-density approximation to f_{xc} do not change qualitatively the results.

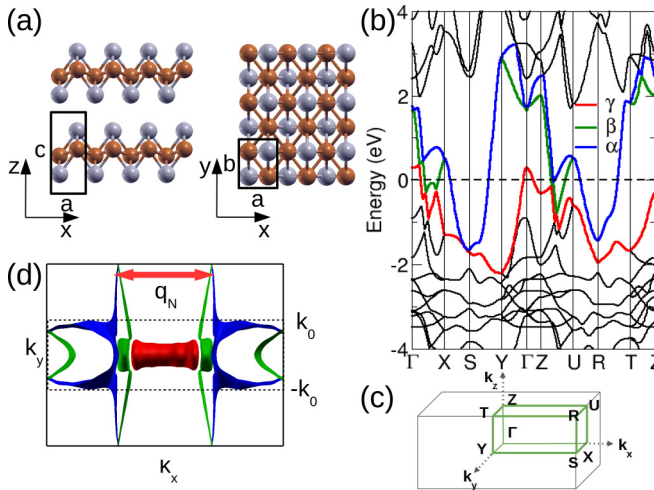


FIG. 1. (a) Different views of the crystal structure of CuTe. In the ball-and-stick representation, brown spheres are Cu atoms and gray spheres are Te atoms. The black rectangle is the projection of the unit cell. (b) Band structure in the orthorhombic Brillouin zone. (c) For the high symmetry \mathbf{k} points we follow the notation of Ref. [20]. The zero of the energy is the Fermi level. (d) Top view of the Fermi surface in the $X-\Gamma-Y$ plane. The dashed lines delimit the two different regions of the FS associated to heavy holes and light electrons, respectively.

III. RESULTS AND DISCUSSION

The crystal structure of CuTe [Fig. 1(a)] is formed by slabs of Te-Cu-Te layers that crystallize in an orthorhombic unit cell consisting of one formula unit of CuTe. In particular, the Cu atoms are arranged in a buckled square lattice encapsulated between two layers of Te atoms which form a rectangular lattice resulting in a quasi-1D chain structure along the a axis.

The electronic band structure [see Fig. 1(b)] displays three dispersive bands crossing the Fermi level (metallic bands) that are weakly hybridized with the other more flat bands below -2 eV. While these fully occupied flat bands originate mostly from Cu d states and are responsible for the in-plane Cu-Cu covalent bonds, the dispersive bands are mainly related to the p and s states of Te. In particular, the most dispersive bands labeled with α and β are dominated by Te p_x (σ bond along the a axis) and p_y (π bond along the a axis) states, respectively. The third band (γ band) presents an sp_z character and a higher hybridization with the Cu d states. However, the hybridization between Te and Cu states is reduced when onsite interactions for the Cu d states are included [21].

The quasi 1D arrangement of the Te atoms causes a strong anisotropy in the dispersion of the metallic bands inside the first Brillouin zone [see Fig. 1(c)]. Indeed, the α and β bands are highly dispersive along the k_x direction with a bandwidth between 3 and 4 eV along the RT and SY symmetry lines and weakly dispersive along the k_y direction where the bandwidth is halved. The dispersion is strongly reduced along the k_z direction as a consequence of the layered structure of the system. The γ band, on the other hand, is characterized by a weaker dispersion due the higher hybridization with the Cu d states that are more localized. Interestingly, the α and β bands lose their quasi-1D character along the ΓX line where

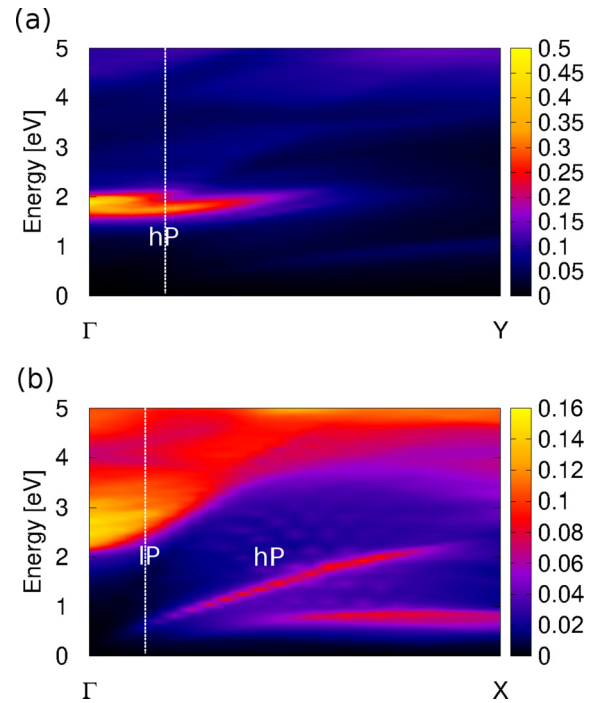


FIG. 2. Loss function of CuTe as a function of momentum transfer (x axis in the plot) along the ΓY direction (a) and the ΓX direction (b). The white dashed lines indicate the cuts of the loss function reported in Fig. 3.

the dispersion becomes similar to that in the k_y direction. This behavior gives rise to a complex Fermi surface (FS) characterized by several branches with different electronic character [see Fig. 1(d)]. In particular, the FS can be split into two main regions. The first one with $|k_y| < k_0$ ($k_0 \approx 2.2 \text{ \AA}^{-1}$) involves all the metallic bands and is characterized by heavy hole pockets with quasi-2D behavior. The second one, on the other hand, involves only the α and β bands with $|k_y| > k_0$ and is characterized by light electron sheets with quasi-1D behavior. This region presents a strong nesting factor at wave vector $\mathbf{q}_N = 0.78 \text{ \AA}^{-1}$ along ΓX which has been associated with the appearance of large Kohn anomalies in the phonon spectra and plays a key role in the CDW phase transition of the system [20,21]. In the following we will analyze the implications of this intriguing electronic structure on the spectra of neutral electronic excitations.

A. High energy collective excitations

Figure 2 shows the loss function of CuTe as a function of in-plane momentum transfer \mathbf{q} , which can be also directly measured by electron energy-loss spectroscopy (EELS). The anisotropy observed in the electronic band structure is reflected in the loss function as well. Indeed, while along the ΓY line [panel (a) in Fig. 2] the spectrum is dominated by a sharp and nondispersive peak at 2 eV, along the ΓX line [panel (b) in Fig. 2] it is characterized by several features with positive dispersion. In particular, besides the main structure at 2.5 eV for $\mathbf{q} \rightarrow 0$, corresponding to a strongly broadened peak, we can clearly distinguish two other well defined peaks at lower energies. The first one has a linear dispersion as a function

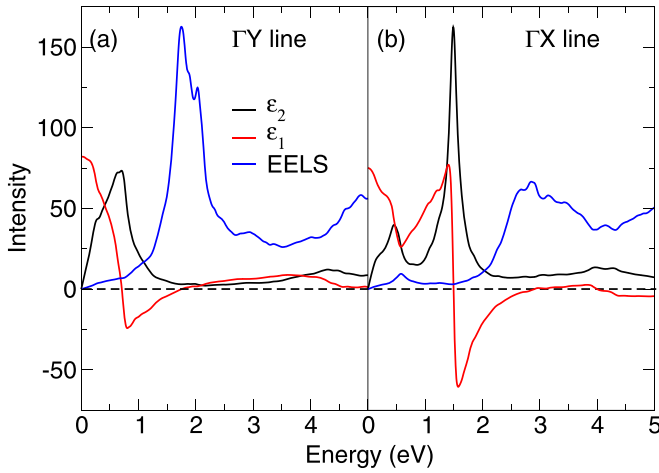


FIG. 3. Real and imaginary parts of the dielectric function and EELS spectrum evaluated at $|q| = 0.15 \text{ \AA}^{-1}$ along the ΓY [panel (a)] and ΓX [panel (b)] symmetry lines. The EELS spectra have been multiplied for a factor 5×10^2 . The wave vector $|q| = 0.15 \text{ \AA}^{-1}$ corresponds to the values $0.20Y$ and $0.16X$ along the ΓY and ΓX symmetry lines, respectively.

of \mathbf{q} and goes to zero in the optical limit. The second one is almost nondispersive and becomes visible only at large \mathbf{q} .

To gain further insight into the nature of these excitations we show in Fig. 3 the real (ϵ_1) and imaginary (ϵ_2) part of the dielectric function. Comparing Fig. 3 and Fig. 2 we can conclude that the main structures in the loss function are plasmon resonances since they correspond to zeros of $\epsilon_1(\mathbf{q}, \omega)$. In particular, the frequency of the non dispersive plasmon along the ΓY line is located just above the peak at 0.6 eV in $\epsilon_2(\mathbf{q}, \omega)$ [see Fig. 3(a)] which is associated with intraband transitions involving heavy-hole-like states with $|k_y| < k_0$. This means that the sharp peak of the loss function in the ΓY direction can be interpreted as a collective excitation of the heavy-hole-like particles with quasi-2D character. In the following, we will call this excitation “heavy plasmon” (hP). Quite different is the situation along ΓX [see Fig. 3(b)]. Here, besides the intraband peak at 0.5 eV related to the heavy-hole states, $\epsilon_2(\mathbf{q}, \omega)$ displays also a more pronounced peak at 1.5 eV . This feature is associated with the intraband transitions between the highly dispersive α and β bands in the $|k_y| > k_0$ sector of the first Brillouin zone, which induces two main effects in the loss function. First, through the Kramers-Kronig relations, it makes ϵ_1 rise very fast at an energy just above the position of the first peak in ϵ_2 so that ϵ_1 does not have zeros at lower energies. As a consequence, the hP is redshifted and strongly damped by independent electron-hole pair transitions. Second, it gives rise to the higher energy plasmon at 2.5 eV . This feature, which in the following we will refer to as “light plasmon” (IP), is a collective excitation of the quasi-1D light particles belonging to the nested region of the FS. Due to its proximity to higher energy interband transitions involving the Cu d states, it is strongly coupled with these excitations and appears as a strongly broadened peak in the loss function. Finally, the weakly dispersive feature at about 0.6 eV in Fig. 2(b) is related to dipole forbidden interband transitions between the

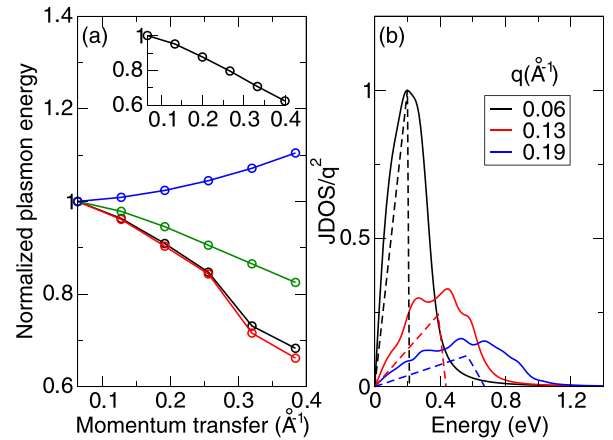


FIG. 4. (a) Plasmon dispersion along the ΓY line for the bare hP of CuTe evaluated in different approximations [i.e., full calculation (black line), neglecting crystal local fields (red line), obtained from the JDOS (green line)] and for the HEG plasmon (blue line). The plasmon energy has been normalized to the energy of the smallest \mathbf{q} . The inset refers to the bare IP along ΓX . (b) $\text{JDOS}(\mathbf{q}, \omega)/|\mathbf{q}|^2$ in CuTe (solid lines) and in the HEG (dashed lines). The intensity has been normalized in order to be the same at the smallest \mathbf{q} .

three metallic bands that become visible at large momentum transfer.

From this analysis, we can conclude that the interplay between quasi-1D and -2D behavior of the conduction electrons in CuTe results in the formation of two kinds of collective excitations namely hP and IP. The latter is visible only along the ΓX line while the former is always visible. However, while along the ΓY line hP is almost nondispersive, along ΓX it is characterized by a linear dispersion typical of acousticlike excitations.

In order to disentangle the behavior of the conduction electrons and understand their role in the measurable EELS spectra, in the calculations we can artificially suppress the interband transitions. The resulting intrinsic plasmon dispersion along ΓY is shown in Fig. 4(a) (black circles). Surprisingly, we find that the hP energy decreases for increasing momentum transfer, i.e., the dispersion is negative [a similar behavior is found for the IP along ΓX shown in the inset of Fig. 4(a)]. This is in striking contrast with respect to the behavior of the layered electron gas (LEG) with infinite number of layers that is often used as a reference system to model collective excitations in layered metallic systems [30]. In this limit the LEG is also equivalent to the homogeneous electron gas (HEG): In both cases the plasmon dispersion in the RPA is positive and parabolic. In the following for simplicity of analysis we will refer to the HEG only.

This remarkable difference with respect to the HEG has been found in other experimental and theoretical works on CDW systems where the unusual negative plasmon dispersion in the direction of the CDW wave vector has been ascribed to the quantum fluctuations associated to the CDW instability [12–14]. However, in the case of CuTe the intrinsic negative plasmon dispersion is present also in the ΓY direction where there is no evidence of any instability. This observation rules out the CDW as possible origin of the plasmon softening

suggesting that the intrinsic negative plasmon dispersion has a completely different nature.

The first possibility is the fact that the electronic charge in CuTe, contrary to the HEG, is spatially inhomogeneous. Thus crystal local-field effects (LFE), which are related to induced short-range spatial charge fluctuations [quantified by the off-diagonal components of the microscopic dielectric function $\epsilon_{\mathbf{G},\mathbf{G}'}^{-1}$ in Eq. (3)], may alter considerably the plasmon dispersion. In Fig. 4(a) we show the intraband plasmon dispersion obtained purposely removing the LFE in CuTe (red circles). By comparing this result with the full calculation (black circles), we can conclude that LFEs play a minor role for the in-plane plasmon properties of CuTe and are not able to change the plasmon dispersion that remains negative.

Therefore the difference with respect to the HEG must reside in the electronic structure of CuTe itself. To pin down the reason of the qualitatively different plasmon properties it is convenient to express ϵ_1 in terms of ϵ_2 through the Kramers-Kronig relations that in the present case take a simpler structure. Indeed, in the absence of interband transitions, as in the case of the HEG, $\epsilon_2 = 0$ above the plasmon frequency and thus ϵ_1 satisfies the relation [31]:

$$\epsilon_1(\mathbf{q}, \omega) = 1 - \frac{2}{\pi} \int_0^\omega d\omega' \frac{\omega' \epsilon_2(\mathbf{q}, \omega')}{\omega^2 - \omega'^2} \quad (6)$$

which is valid for ω close to ω_p^b (ω_p^b being the “bare” plasmon frequency obtained removing the interband transitions). The frequencies $\omega_p^b = \omega_p^b(\mathbf{q})$ for which $\epsilon_1(\mathbf{q}, \omega_p^b) = 0$ define the plasmon dispersion. Moreover, in the HEG ϵ_2 is proportional to the joint density of states (JDOS): $\epsilon_2(\mathbf{q}, \omega) \propto \text{JDOS}(\mathbf{q}, \omega)/|\mathbf{q}|^2$. Here the presence of a wide parabolic energy band gives rise to a sharp peak in the JDOS with strong positive dispersion with \mathbf{q} [see Fig. 4(b)]. In turn, the integral in Eq. (6) is an increasing function of \mathbf{q} , and the zeros of ϵ_1 are shifted to higher frequencies progressively with \mathbf{q} ($\epsilon_1 < 0$ for $\omega \lesssim \omega_p^b$). The resulting plasmon [blue circles in Fig. 4(a)] has a positive dispersion. A completely different behavior is found in CuTe. Indeed, in this case the JDOS is strongly broadened due to the appearance of new features below the main peak as \mathbf{q} increases [see Fig. 4(b)]. They are related to the transitions between different bands crossing the Fermi level or different sheets of the FS that are activated at finite \mathbf{q} and are always present as the electronic band structure departs from the free electron dispersion. The broadening results in a reduction of the amount of spectral weight transferred to the high frequency region. Under these conditions, if the main peak in the JDOS is not dispersive enough, the integral in Eq. (6) will be a decreasing function of \mathbf{q} . This is just what happens in CuTe. As a matter of fact, using the JDOS of CuTe in Eq. (6), we can calculate ϵ_1 and its zero crossing that defines the plasmon frequency when the oscillator-strength matrix elements (ME) are neglected in Eq. (5). As we can see from the green circles in Fig. 4(a), the plasmon dispersion is still negative demonstrating that the intrinsic negative plasmon dispersion in this system is a pure band structure effect. This behavior is common to other CDW systems such as metallic TMDs [31,32] as well as materials that do not display CDW instability [33] such as doped molecular crystals [34] and electrides [35]. In other words there is no correlation between

plasmon softening and CDW instability. On the contrary, as we will discuss in the next section, the quantum fluctuations of the CDW can be related with the low energy incoherent part of the EELS spectra.

Finally, the higher energy interband transitions above the plasmon frequency induce an effective screening on the long range part of the Coulomb interaction responsible for the collective excitations [36]. As a consequence, in a first approximation, their effect on the intraband plasmon can be modeled through a renormalization of the bare plasmon frequency. Thus the full plasmon frequency becomes: $\omega_P(\mathbf{q}) \approx \omega_p^b(\mathbf{q})/\sqrt{\epsilon_0(\mathbf{q})}$, where ϵ_0 is a background dielectric constant associated with the interband transitions. Its effect is twofold: (i) a redshift of the plasmon frequency; (ii) a reduction of the intrinsic negative plasmon dispersion related to the fact that ϵ_0 is a decreasing function of \mathbf{q} . In particular, due to the proximity of the interband transitions to the plasmon energy along the ΓX line, screening effects are particularly strong on the IP so that the slope of its dispersion switches to a positive value. Along the ΓY line, on the other hand, the screening is weaker and its effect is to suppress the intrinsic negative dispersion of the hP without changing its slope. It is important to note that along the ΓX line the hP is screened also in the absence of interband transitions due to the intraband transitions between light electron states associated to the α and β bands. This metallic screening that diverges as $1/|\mathbf{q}|^2$ for $\mathbf{q} \rightarrow 0$ is responsible for the linear acousticlike dispersion of the hP in the optical limit. Acoustic plasmons have been theorized by Pines [23], who showed that they can occur in a two-component electron plasma consisting of “slow” and “fast” carriers. The latter can act to screen the repulsion between the former, resulting in the appearance of a plasma mode with a soundlike dispersion. This is, for instance, what has been proved in MgB₂ [37], which has two bands with π (fast carriers) and σ (slow carriers) character that are metallic or in other materials such as CaC₆ [38], Pb [39], and Pd [40]. In the present case, the two-component electron plasma consists of quasi-2D heavy-hole-like states and quasi-1D light-electron states that play the role of the “slow” and “fast” carriers, respectively.

Being a layered material, CuTe is expected to exhibit anisotropic electronic properties along the c axis. To validate this expectation, we have also calculated the loss function for momentum transfers \mathbf{q} perpendicular to the Te-Cu-Te layers. Figure 5(a) shows that a low-energy plasmon, corresponding to the collective excitation of the heavy-hole states, is present also for the out-of-plane direction at 0.4 eV. It shows almost no dispersion at all, in analogy with its counterpart along ΓY . In contrast to the in-plane spectra, where the collective modes are restricted to a small fraction of momentum space (see Fig. 2), in this case the plasmon peak is a long-lived feature that remains visible also for \mathbf{q} well beyond the first Brillouin zone. However, in the spectra calculated without LFE [see Fig. 5(b)] the plasmon peak fades away already within the first Brillouin zone. We hence realize that the long-lived character of the plasmon is a direct consequence of the strong LFE due to the strong charge inhomogeneities normal to the layers. It is a distinctive feature that plasmons in different layered materials like MgB₂ [41], graphite [42], TMDs [31,32], and electrides [35] all have in common. The mechanism behind

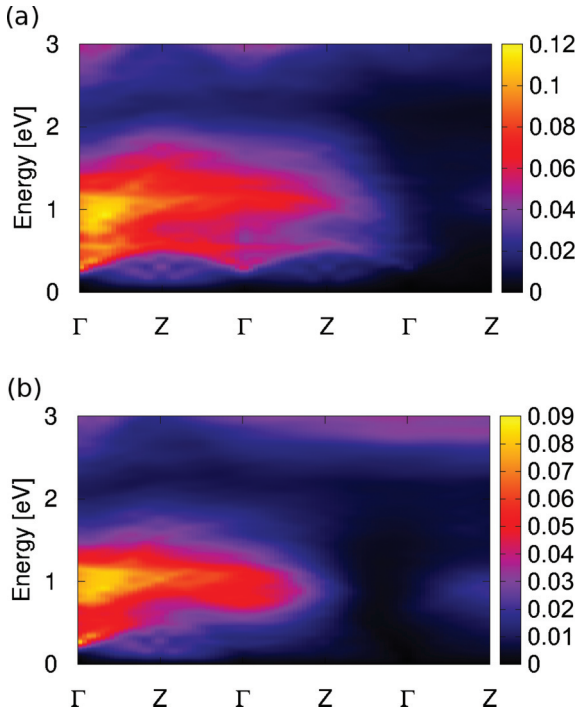


FIG. 5. Loss function of CuTe as a function of momentum transfer (x axis in the plot) along the Γ Z direction up to third Brillouin zone calculated (a) with and (b) without local fields.

the reappearance of the first-Brillouin-zone spectra at larger momentum transfers can be explained within a two-plasmon-band model [43]. As a matter of fact, off-diagonal elements of the dielectric matrix, i.e., LFE, are responsible for the coupling between independent electron-hole excitations at large \mathbf{q} and the first-Brillouin-zone plasmon, inducing its persistence in the spectra also in other Brillouin zones.

B. Low energy excitations and their link with the CDW instability

So far we analyzed the behavior of the collective plasmonic excitations of CuTe demonstrating that there is not a direct link between the plasmon dispersion and the CDW instability. However, previous studies pointed out that, even though the driving force of the CDW phase transition is the electron-phonon interaction, also the electron-electron scattering by FS nesting of the quasi-1D Te p orbitals plays a key role in the phonon softening.

Therefore, a natural question arises: What is the effect of these scattering processes on the spectra of neutral electronic excitations? To answer this question, in the following we will focus on the low energy region of the loss function where the spectrum is dominated by transitions among the three metallic bands involved in the CDW pairing.

Figure 6 shows the low energy region of the loss function along the Γ X symmetry line for different values of the momentum transfer around \mathbf{q}_N . At small \mathbf{q} , above 0.1 eV, the spectra do not show any structure. However, as the momentum transfer approaches the nesting $\mathbf{q}_N = 0.78 \text{ \AA}^{-1}$, a shoulder appears at 0.32 eV and remains visible up to $\mathbf{q} \approx \mathbf{q}_N$. Since in this energy region ϵ_1 is almost frequency independent, the

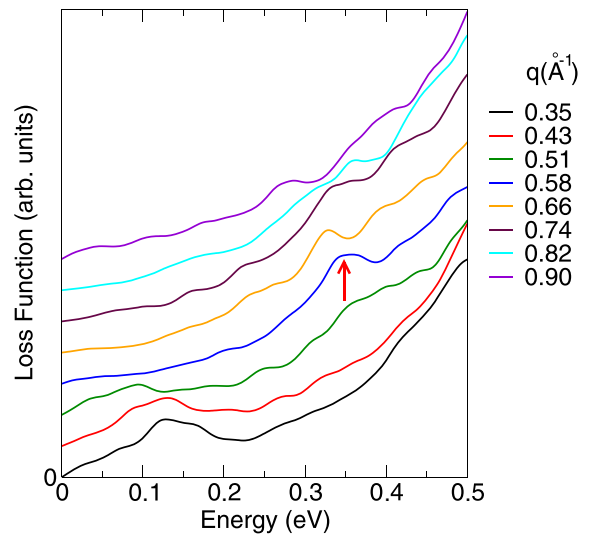


FIG. 6. Low energy region of the loss function for different values of the momentum transfer around \mathbf{q}_N in the Γ X direction. The red arrow indicates the position of the shoulder. Each curve has a vertical offset for clarity reasons.

different features of the loss function are directly related to the peaks of ϵ_2 that define the incoherent part of the EELS spectra [see Eq. (1)]. Thus, the nature of the shoulder can be directly understood by analyzing the structure of the imaginary part of the dielectric function. In Fig. 7(a), indeed, the shoulder is clearly visible in ϵ_2 as well. It is located below the main peak at 0.6 eV that is related to the interband transitions between metallic bands which are responsible for the appearance of a non dispersive feature in the loss function at large \mathbf{q} [see Fig. 2(b)].

From the decomposition of ϵ_2 into the different contributions arising from the three metallic bands, we can conclude that the shoulder is related to the electron-hole pairs belonging

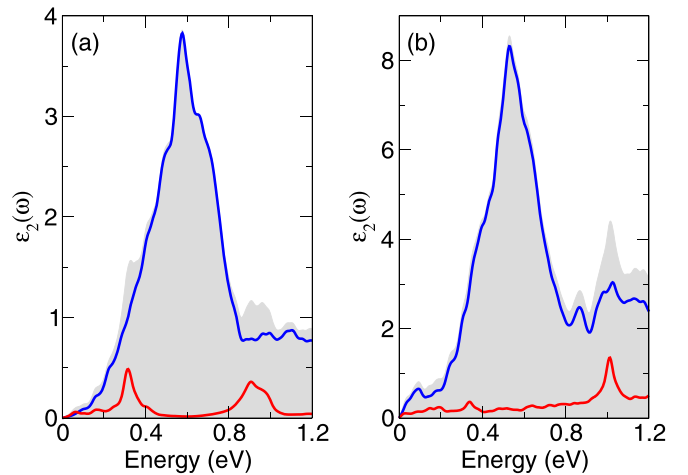


FIG. 7. Imaginary part of the dielectric function evaluated at $\mathbf{q} = 0.74 \text{ \AA}^{-1}$ (a) and $\mathbf{q} = 0.51 \text{ \AA}^{-1}$ (b). The gray region defines the full spectrum while the red line is the contribution from intraband transitions of the α and β bands. The blue line is the remaining contribution.

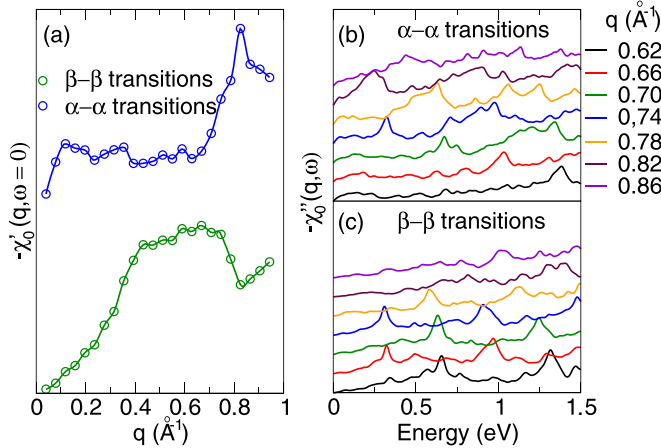


FIG. 8. Real part of the static Lindhard function as a function of the momentum transfer along ΓX (a) and imaginary part of the dynamical Lindhard function for different values of the momentum transfer along ΓX for the α (b) and β (c) bands.

to the nested bands α and β [red curve in Fig. 7(a)]. Moreover, at smaller \mathbf{q} [see Fig. 7(b)] the contribution of these bands is blueshifted and results hidden by the dominant peak. As a consequence the shoulder disappears. This demonstrates that the appearance of the shoulder in the loss function at large \mathbf{q} is due to the progressive redshift of a peak in ϵ_2 associated to neutral excitations involving the nested bands. This behavior does not change when both ME and crystal LFE are neglected in the calculation of ϵ_2 suggesting that it is a pure band effect. In the following we will show that this behavior is tightly linked with the CDW instability.

In a simplified independent particle picture, the CDW transition can be understood in terms of the Lindhard function χ_0 evaluated in the static limit ($\omega \rightarrow 0$). In our computational framework it can be directly obtained neglecting the ME in Eq. (5). In particular, the imaginary part of χ_0 (χ_0'') reflects the FS topology and allows one to quantify the FS nesting through the evaluation of the nesting factor at a given \mathbf{q} (i.e., the quantity $\lim_{\omega \rightarrow 0} \chi_0''(\mathbf{q}, \omega)/\omega$), while the real part (χ_0') gives information about the stability of the system (i.e., a divergence of χ_0' at some \mathbf{q} could result in the formation of a CDW). For both quasi-1D bands α and β , $\chi_0'(\mathbf{q}, \omega = 0)$ displays peaks for $0.6 \text{ \AA}^{-1} < \mathbf{q} < 0.8 \text{ \AA}^{-1}$ [see Fig. 8(a)]. The strongest one occurs at $\mathbf{q} \approx \mathbf{q}_N$ (i.e., in proximity of a peak in the nesting factor) for the α band and for this reason it has been ascribed to the FS nesting.

Moreover, as shown in Refs. [20,21], it is responsible for the appearance of large Kohn anomalies in the phonon band structure. Interestingly, as we can infer from Fig. 8(b), the progressive increase of $\chi_0'(\mathbf{q}, \omega = 0)$ as $\mathbf{q} \rightarrow \mathbf{q}_N$ is accompanied by the redshift (or softening) of peaks in the spectrum of $\chi_0''(\mathbf{q}, \omega)$ which is associated to the presence of high density electron-hole pairs whose energy decreases as their wave vector approaches \mathbf{q}_N . This is the physical origin of the shoulder observed in ϵ_2 . Indeed, when ME and crystal LFE are neglected, $\epsilon_2(\mathbf{q}, \omega) = -\frac{4\pi}{|\mathbf{q}|^2} \chi_0''(\mathbf{q}, \omega)$.

The correlation between the behavior of χ_0' and the neutral excitations can be understood expressing χ_0' in terms of χ_0

through the Kramers-Kronig relation:

$$\chi_0'(\mathbf{q}, \omega = 0) = \frac{2}{\pi} \int_0^\infty \frac{\chi_0''(\mathbf{q}, \omega')}{\omega'} d\omega'. \quad (7)$$

As pointed out also in Refs. [6,7], the behavior of $\chi_0'(\mathbf{q}, \omega = 0)$ is set not only by the nesting factor but also by the whole spectrum of χ_0'' . In general, a negative dispersive peak in $\chi_0''(\mathbf{q}, \omega)$ causes a transfer of spectral weight to lower frequencies and will result in an enhancement of $\chi_0'(\mathbf{q}, \omega = 0)$. Thus, a peak in χ_0' at some \mathbf{q} should be associated to both Kohn anomalies in the phonon spectra as well as to the presence of high density electron-hole pairs whose energy decreases as their wave vector approaches \mathbf{q} . These excitations give rise to negative dispersive features in the incoherent part of the EELS spectra. In particular, when the energy of these excitations goes to zero, $\chi_0''(\mathbf{q}, \omega = 0)$ takes a finite value and $\chi_0'(\mathbf{q}, \omega = 0)$ diverges. This is just what happens in the case of the 1D electron gas that in an independent particle picture is electronically unstable.

It is important to note that in an interacting system an electronic instability corresponds to a divergence of the the real part of the full charge-charge response function χ' instead of χ_0' . This means that the system is characterized by peaks in χ'' (i.e., neutral excitations related to the superposition of interacting electron-hole pairs) that soften at a given wave vector. In principle, being χ' bound by the Coulomb potential [see Eq. (4)], it could remain finite even if χ_0' diverges. In other words, in real materials the complete softening of a finite number of neutral electronic excitations is prevented by the repulsive Coulomb potential. Under these conditions the system is electronically stable even if χ_0' diverges or presents a strong peak at some \mathbf{q} and the electron-phonon interaction plays a key role in setting the CDW phase transition also called Peierls distortion. Moreover, the enhancement of $\chi_0'(\mathbf{q}, \omega = 0)$ is directly linked to the appearance of peaks in the low energy region of the loss function. This is just the case of CuTe. However, in the alternative scenario namely excitonic insulator, exchange-correlation effects beyond the RPA could induce a complete softening of electronic excitations at some \mathbf{q} . These excitations are associated to a peak in the low energy region of the loss function characterized by negative dispersion whose energy goes to zero at wave vector close to \mathbf{q} [14,18]. In this case χ' diverges and the CDW is stabilized also without electron-phonon interaction. Our study suggests that the presence of negative dispersive peaks in the low energy region of the loss function is a feature common to both mechanisms. The difference is actually only quantitative. While in the excitonic insulator the energy of the negative dispersive peak goes to zero at the CDW wave vector, in the Peierls distortion it reaches a finite value and the system is electronically stable in absence of electron-phonon interaction.

IV. CONCLUSIONS

In summary, we performed an extensive study of neutral electronic excitations in CuTe through first-principles calculation of the loss function. We have shown that the intrinsic negative plasmon dispersion in this material is a pure band effect common to other CDW systems as well as to systems

that do not display CDW order. This behavior can occur when the electronic band structure departs from that of the homogeneous electron gas as a consequence of the confinement of the electronic wave functions and multiband effects. Therefore there is no correlation between plasmon softening and CDW instability. On the other hand, the CDW instability is tightly linked with the presence of negative dispersive structures in the incoherent part of the loss function involving incoherent electron-hole pairs superpositions such as excitons and resonant excitations that occur together with the phonon softening. This is a feature common to both excitonic insulators and Peierls unstable systems that further highlight how the difference between the two scenarios is at most quantitative [17,44,45]. While in the excitonic insulator the energy of the negative dispersive peak goes to zero at the CDW wave vector, in the Peierls distortion it reaches a finite value. This different quantitative behavior can be used to disentangle the two mechanisms.

In addition, we predicted the existence of an acoustic plasmon for momentum transfer along the ΓX symmetry line. This is a peculiarity of CuTe and is related to the coexistence of electronic states with quasi-2D and quasi-1D character that behave as “slow” and “fast” carriers, respectively. According to Pines’ theory [23], the latter screen the repulsion between the former, resulting in the appearance of a plasmon mode with a soundlike dispersion. Finally, we have predicted the plasmon dispersion along the direction perpendicular to the layers, with the reappearance around Bragg reflections of the plasmon of the first Brillouin zone.

ACKNOWLEDGMENT

This research was supported by the Fonds National de Recherche (FNR), Luxembourg, via project INTER/19/ANR/13376969/ACCEPT.

-
- [1] G. Grüner, *Density Waves in Solids* (Addison-Wesley, 1994).
 - [2] K. Rossnagel, *J. Phys.: Condens. Matter* **23**, 213001 (2011).
 - [3] J. A. Wilson, F. J. Di Salvo, and S. Mahajan, *Phys. Rev. Lett.* **32**, 882 (1974).
 - [4] T. M. Rice and G. K. Scott, *Phys. Rev. Lett.* **35**, 120 (1975).
 - [5] D. Jérôme, T. M. Rice, and W. Kohn, *Phys. Rev.* **158**, 462 (1967).
 - [6] M. D. Johannes, I. I. Mazin, and C. A. Howells, *Phys. Rev. B* **73**, 205102 (2006).
 - [7] M. D. Johannes and I. I. Mazin, *Phys. Rev. B* **77**, 165135 (2008).
 - [8] A. Wegner, J. Zhao, J. Li, J. Yang, A. A. Anikin, G. Karapetrov, K. Esfarjani, D. Louca, and U. Chatterjee, *Phys. Rev. B* **101**, 195145 (2020).
 - [9] R. E. Peierls, *Quantum Theory of Solids* (Clarendon Press, Oxford, 1955).
 - [10] W. Kohn, *Phys. Rev. Lett.* **2**, 393 (1959).
 - [11] E. Tosatti, and R. Girlanda, *Plasmons in Layered Compounds. Electronic Structure and Electronic Transitions in Layered Materials* (Springer, Dordrecht, 1986), p. 461.
 - [12] J. van Wezel, R. Schuster, A. König, M. Knupfer, J. van den Brink, H. Berger, and B. Büchner, *Phys. Rev. Lett.* **107**, 176404 (2011).
 - [13] R. Schuster, R. Kraus, M. Knupfer, H. Berger, and B. Büchner, *Phys. Rev. B* **79**, 045134 (2009).
 - [14] A. Kogar, M. S. Rak, S. Vig, A. A. Husain, F. Flicker, Y. I. Joe, L. Venema, G. J. MacDougall, T. C. Chiang, E. Fradkin, J. van Wezel, and P. Abbamonte, *Science* **358**, 1314 (2017).
 - [15] W. Kohn, *Phys. Rev. Lett.* **19**, 439 (1967).
 - [16] D. Varsano, S. Sorella, D. Sangalli, M. Barborini, S. Corni, E. Molinari, and M. Rontani, *Nat. Commun.* **8**, 1461 (2017).
 - [17] D. Pasquier and O. V. Yazyev, *Phys. Rev. B* **98**, 235106 (2018).
 - [18] C. Lian, Z. A. Ali, and B. M. Wong, *Phys. Rev. B* **100**, 205423 (2019).
 - [19] Z. Jiang, W. Lou, Y. Liu, Y. Li, H. Song, K. Chang, W. Duan, and S. Zhang, *Phys. Rev. Lett.* **124**, 166401 (2020).
 - [20] K. Zhang, I. X. Liu, H. Zhang, K. Deng, M. Yan, W. Yao, M. Zheng, E. F. Schwier, K. Shimada, J. D. Denlinger, Y. Wu, W. Duan, and S. Zhou, *Phys. Rev. Lett.* **121**, 206402 (2018).
 - [21] S. Kim, B. Kim, and K. Kim, *Phys. Rev. B* **100**, 054112 (2019).
 - [22] F. Aryasetiawan and K. Karlsson, *Phys. Rev. Lett.* **73**, 1679 (1994).
 - [23] D. Pines, *Can. J. Phys.* **34**, 1379 (1956).
 - [24] G. Onida, L. Reining, and A. Rubio, *Rev. Mod. Phys.* **74**, 601 (2002).
 - [25] E. Runge and E. K. U. Gross, *Phys. Rev. Lett.* **52**, 997 (1984).
 - [26] W. Kohn and L. J. Sham, *Phys. Rev.* **140**, A1133 (1965).
 - [27] P. Giannozzi, S. Baroni, N. Bonini, M. Calandra, R. Car, C. Cavazzoni, D. Ceresoli, G. L. Chiarotti, M. Cococcioni, and I. Dabo, *J. Phys.: Condens. Matter* **21**, 395502 (2009).
 - [28] D. R. Hamann, *Phys. Rev. B* **88**, 085117 (2013).
 - [29] A. Marini, C. Hogan, M. Grüning, and D. Varsano, *Comput. Phys. Commun.* **180**, 1392 (2009).
 - [30] M. Eto, *J. Phys. Soc. Jpn.* **63**, 229 (1994).
 - [31] P. Cudazzo, M. Gatti, and A. Rubio, *Phys. Rev. B* **86**, 075121 (2012).
 - [32] P. Cudazzo, M. Gatti, and Angel Rubio, *Phys. Rev. B* **90**, 205128 (2014).
 - [33] P. Cudazzo, E. Müller, C. Habenicht, M. Gatti, H. Berger, M. Knupfer, A. Rubio, and S. Huotari, *New J. Phys.* **18**, 103050 (2016).
 - [34] P. Cudazzo, M. Gatti, F. Roth, B. Mahns, M. Knupfer, and A. Rubio, *Phys. Rev. B* **84**, 155118 (2011).
 - [35] P. Cudazzo and M. Gatti, *Phys. Rev. B* **96**, 125131 (2017).
 - [36] P. Cudazzo, M. Gatti, and Angel Rubio, *New J. Phys.* **15**, 125005 (2013).
 - [37] V. M. Silkin, A. Balassis, P. M. Echenique, and E. V. Chulkov, *Phys. Rev. B* **80**, 054521 (2009).
 - [38] J. P. Echeverry, E. V. Chulkov, P. M. Echenique, and V. M. Silkin, *Phys. Rev. B* **85**, 205135 (2012).
 - [39] X. Zubizarreta, V. M. Silkin, and E. V. Chulkov, *Phys. Rev. B* **87**, 115112 (2013).
 - [40] V. M. Silkin, I. P. Chernov, Yu. M. Koroteev, and E. V. Chulkov, *Phys. Rev. B* **80**, 245114 (2009).
 - [41] Y. Q. Cai, P. C. Chow, O. D. Restrepo, Y. Takano, K. Togano, H. Kito, H. Ishii, C. C. Chen, K. S. Liang, C. T. Chen, S. Tsuda,

- S. Shin, C. C. Kao, W. Ku, and A. G. Eguiluz, *Phys. Rev. Lett.* **97**, 176402 (2006).
- [42] R. Hambach, C. Giorgetti, F. Sottile, L. Reining, N. Hiraoka, Y. Q. Cai, A. G. Marinopoulos, and F. Bechstedt, *Phys. Rev. Lett.* **101**, 266406 (2008).
- [43] L. E. Oliveira and K. Sturm, *Phys. Rev. B* **22**, 6283 (1980).
- [44] J. van Wezel, P. Nahai-Williamson, and S. S. Saxena, *Phys. Rev. B* **81**, 165109 (2010).
- [45] B. A. Volkov, Y. V. Kopaev, and A. I. Rusinov, Sov. Phys. JETP **41**, 952 (1975).